


RESEARCH ARTICLE

Open Access



Amide chemical exchange saturation transfer at 7 T: a possible biomarker for detecting early response to neoadjuvant chemotherapy in breast cancer patients

Erwin Krikken^{1*} , Vitaliy Khlebnikov¹, Moritz Zaiss², Rajni A. Jibodh³, Paul J. van Diest⁴, Peter R. Luijten¹, Dennis W. J. Klomp¹, Hanneke W. M. van Laarhoven³ and Jannie P. Wijnen¹

Abstract

Background: The purpose of this work was to investigate noninvasive early detection of treatment response of breast cancer patients to neoadjuvant chemotherapy (NAC) using chemical exchange saturation transfer (CEST) measurements sensitive to amide proton transfer (APT) at 7 T.

Methods: CEST images were acquired in 10 tumors of nine breast cancer patients treated with NAC. APT signals in the tumor, before and after the first cycle of NAC, were quantified using a three-pool Lorentzian fit of the z-spectra in the region of interest. The changes in APT were subsequently related to pathological response after surgery defined by the Miller-Payne system.

Results: Significant differences ($P < 0.05$, unpaired Mann-Whitney test) were found in the APT signal before and after the first cycle of NAC in six out of 10 lesions, of which two showed a pathological complete response. Of the remaining four lesions, one showed a pathological complete response. No significant difference in changes of APT signal were found between the different pathological responses to NAC treatment ($P > 0.05$, Kruskal-Wallis test).

Conclusions: This preliminary study shows the feasibility of using APT CEST magnetic resonance imaging as a noninvasive biomarker to assess the effect of NAC in an early stage of NAC treatment of breast cancer patients.

Trial registration: Registration number, NL49333.041.14/NTR4980. Registered on 16 October 2014.

Keywords: 7 T MRI, APT CEST, NAC treatment, Breast cancer, Response prediction

Background

Neoadjuvant chemotherapy (NAC) is a systemic therapy that downstages cancer, enabling breast-conserving surgery and reducing axillary treatment [1–4]. Unfortunately, patients undergoing NAC may experience severe side effects and, in approximately 20% of patients, treatment does not result in tumor size reduction [5, 6]. To spare patients from ineffective treatment, it would be beneficial to predict the pathological response early in the course of treatment, allowing adjustments for patient-specific therapy.

Currently, the effect of NAC is generally evaluated based on change in the size of the tumor. Since underlying tumor changes in response to treatment usually precede a relatively slow process of change in tumor size [7–9], we set out to investigate metabolic properties of breast cancers that are expected to reveal changes early in the course of treatment.

Image contrast in standard clinical magnetic resonance imaging (MRI) is based on the concentration of water protons, and T_2 - and T_1 -weighted imaging reveal anatomical information of different tissues. A recently developed MRI method, chemical exchange saturation transfer (CEST), allows detection of interactions between metabolites and water in the body [10, 11].

* Correspondence: e.krikken@umcutrecht.nl

¹Department of Radiology, University Medical Center Utrecht, Utrecht, The Netherlands

Full list of author information is available at the end of the article



Amide proton transfer (APT) CEST MRI detects the transfer of magnetization of labeled amide protons (resonating at 3.5 ppm downfield from the water) [12] and is sensitive to cellular mobile protein content as well as tissue pH. NAC treatment may cause an effect on these properties; therefore, we expect to observe changes in APT early in the course of treatment which can be predictive of the pathological response. Dula et al. also assessed the reproducibility of APT imaging in breast cancer patients at 3 T and showed group changes in APT during NAC, suggesting it may predict treatment response [13]. Going to higher field strength (7 T) will improve the signal to noise ratio (SNR) and contrast to noise ratio (CNR), improving the sensitivity of APT signals to therapeutic response [14]. Furthermore, endogenous T_1 relaxation times become longer with increasing field strength, resulting in an increase in CEST signals [15–18].

A few studies have shown reproducible methods which maximize the SNR for APT CEST MRI in the breast at 7 T. They measured the APT effect with a standard deviation of 1% in healthy glandular tissue [14, 19]. Assuming approximately the same standard deviation in tumor tissue, in this preliminary study we set out to investigate the possibility of using personalized APT MRI at 7 T to evaluate the effect of NAC treatment in a cohort of nine breast cancer patients.

Methods

Subjects

This MRI study was performed in accordance with the guidelines of the UMC Utrecht ethics committee and was part of a larger study. Nine breast cancer patients with a total of 10 lesions gave informed consent to participate in this study. Patients being treated with NAC were selected, and they were examined with APT CEST MRI before (pre-) and after (post-) the first cycle of NAC (at approximately 3-week intervals). Table 1 summarizes their demographic and tumor characteristics.

Acquisition

All patients were scanned in a prone position on a 7 T MR system (Philips, Cleveland, OH, USA). Six patients were scanned with a 26-channel bilateral breast ^1H transceiver coil (MR Coils, Zaltbommel, The Netherlands) [20] and three patients were scanned with a 2-channel unilateral $^1\text{H}/^{31}\text{P}$ dual-tuned transceiver coil (MR Coils, Zaltbommel, The Netherlands) [21]. Two setups were used because this was a multicenter study and the RF coil was different in the two facilities. Third-order image-based B_0 shimming was performed with least square error optimization using a 3D B_0 map followed by manual segmentation of the breasts [22].

CEST-MRI was performed using a series of 20 sinc-Gauss radiofrequency (RF) pulses (pulse duration: 100 ms; inter pulse delay: 100 ms; the peak amplitude $B_1 \approx 2 \mu\text{T}$) resulting in a 4-s saturation train (50% duty cycle) followed by a gradient-echo readout [23]. Image acquisition included fat suppression with a short 1–2–1 spectral-spatial RF pulse to allow for a short TE of 1.4 ms, a TR of 2.6 ms, and a flip angle of 1.2° . A coronal field of view (FOV) of $150 \times 320 \times 100 \text{ mm}^3$ (FH \times RL \times AP) with a true resolution of $2.3 \times 3.0 \times 6.8 \text{ mm}^3$ was obtained in two shots with an interval of 4.48 s and a fourfold acceleration in the right-left direction; 33 frequency offsets were acquired resulting in a scan time of 4 min 55 s. These offsets were not equally distributed over the frequencies; more offsets were obtained around the amide peak (3.5 ppm) and the water peak (0.0 ppm) for better fitting of these resonances. The frequency offsets associated with the nuclear Overhauser effect (NOE) were not included due to signal distortions by unsuppressed lipid resonances.

In the same MRI session, the last acquired scan was a dynamic contrast-enhanced (DCE) series. The first high-resolution scan after contrast administration was used to aid delineating the tumor on the CEST images. The dynamic series consisted of 18 consecutive 3D T_1 -weighted gradient echo sequences, starting with a fat-suppressed high-resolution scan prior to the contrast injection of 0.1 mmol/kg gadobutrol (Bayer Schering Pharma AG, Berlin, Germany), followed by 12 high-temporal resolution scans (TE = 1.6 ms, TR = 4.8 ms, flip angle = 8° , FOV = $160 \times 350 \times 160 \text{ mm}^3$, resolution = $2.86 \times 2.86 \times 2.86 \text{ mm}^3$) to finish with another five fat-suppressed high-resolution scans (TE = 2.5 ms, TR = 5.6 ms, flip angle = 8° , FOV = $160 \times 350 \times 160 \text{ mm}^3$, resolution = $0.7 \times 0.7 \times 0.7 \text{ mm}^3$).

Data analysis

Image processing and data analysis were performed with MATLAB 2014b (MathWorks, Natick, MA, USA). CEST images were B_0 corrected using the WASSR method [24]. A region of interest (ROI) was drawn in the whole tumor using the MR image of the last offset (33.6 ppm) of the CEST series before and after the first NAC. The procedure for selecting the ROI in the tumor can be seen in the upper part of Fig. 1 for one single slice. Figure 1a shows the DCE images which were used to aid in selecting the tumor region. The S_0 image acquired at 33.6 ppm (Fig. 1b) was used to draw the ROI in the tumor (the green circle in Fig. 1b). To obtain a mean APT signal in the whole tumor, this procedure was performed for all the slices containing the tumor. The mean APT signal in the ROI, as a function of the frequency (z-spectra), was fitted with a three-pool Lorentzian model (water, APT, and magnetization transfer

Table 1 Patient demographics and tumor characteristics

Patient	Age (years)	Treatment regimes	ER	PR	HER2 neu	Diameter (mm) ^a	TNM stage
1	61	4×AC–12×paclitaxel	+	–	+	24	T2N1M0
2	50	3×FEC–3×docetaxel	+	+	–	30	T4N1M0
3R	57	3×FEC–3×docetaxel	+	+	–	35	T2N0M0
3L	57	3×FEC–3×docetaxel	+	+	–	15	T1N0M0
4	43	3×FEC–3×docetaxel	+	–	–	24	T2N0M0
5	59	3×FEC–3×docetaxel	+	+	–	32	T2N1M0
6	39	3×FEC–3×docetaxel	+	–	–	110	T3N2M0
7	55	6×Taxotere–AC	–	–	–	32	T2N0Mx
8	63	6×Taxotere–AC	+	+	–	15	T2N1Mx
9	35	6×Taxotere–AC	–	–	–	30	T2N0M0

AC adriamycin and cyclophosphamide, ER estrogen receptor, FEC 5-fluorouracil, epirubicin, and cyclophosphamide, HER2 human epidermal growth factor receptor 2, L left, PR progesterone receptor, R right, TNM tumor, nodes, metastasis (classification of malignant tumors)

^a Measurement performed on 3 T magnetic resonance imaging acquired for standard clinical practice

(MT)) using the Levenberg-Marquardt algorithm (see Table 2 for fit parameters [16, 25]):

$$\frac{M_z(\Delta\omega)}{M_z^0(\Delta\omega)} = Z(\Delta\omega) = Z_{base} - \sum_i L_i(\Delta\omega) \tag{1}$$

with

$$L_i(\Delta\omega) = A_i \frac{\Gamma_i^2 / 4}{\Gamma_i^2 / 4 + (\Delta\omega - \delta_i)^2} \tag{2}$$

Each Lorentzian function L_i of effect i is defined for the offset frequency $\Delta\omega$ by amplitude A_i , full width at

half maximum Γ_i , and displacement from the frequency of free water protons δ_i . The parameter Z_{base} corrects for constant signal reduction. The calculated APT map was obtained using the amplitude of the fit of the APT signal. To facilitate the comparison of different lesions in terms of APT signal change following the first NAC cycle, the mean APT signal pre-NAC was normalized to 1. The whole tumor analysis was compared to a single-slice approach containing the largest diameter of the tumor.

Pathology

The pathological responses to NAC are defined according to the Miller-Payne system [26]; complete response is classified as grade 5 and nonresponse as grade 1. Pathological

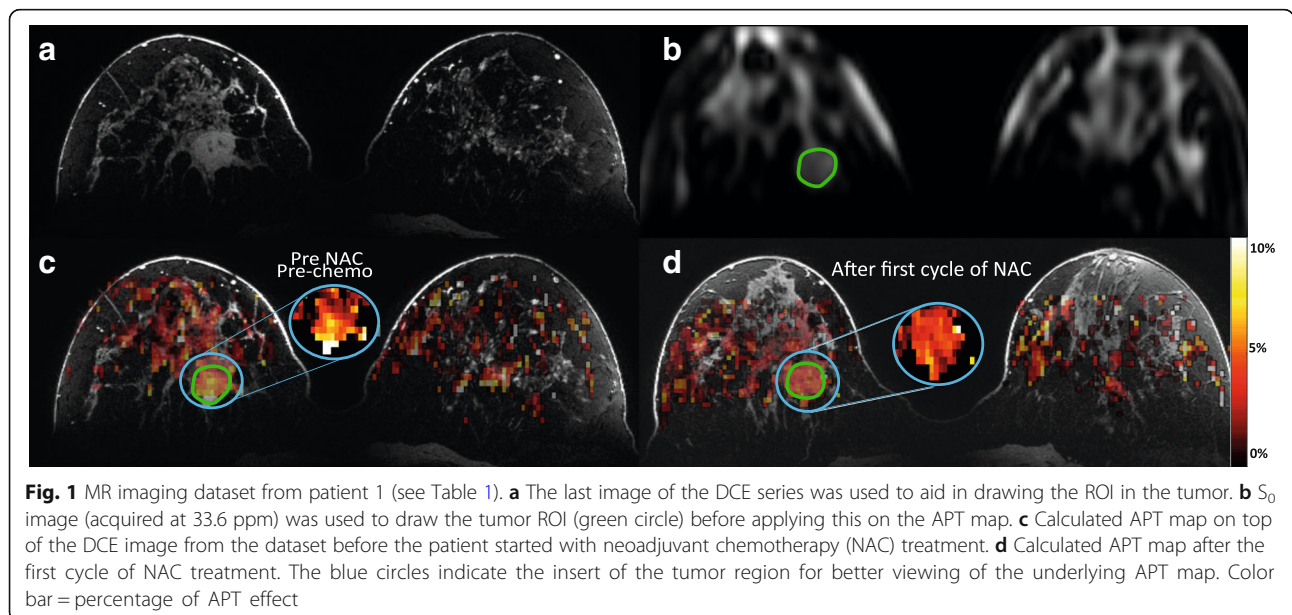


Fig. 1 MR imaging dataset from patient 1 (see Table 1). **a** The last image of the DCE series was used to aid in drawing the ROI in the tumor. **b** S_0 image (acquired at 33.6 ppm) was used to draw the tumor ROI (green circle) before applying this on the APT map. **c** Calculated APT map on top of the DCE image from the dataset before the patient started with neoadjuvant chemotherapy (NAC) treatment. **d** Calculated APT map after the first cycle of NAC treatment. The blue circles indicate the insert of the tumor region for better viewing of the underlying APT map. Color bar = percentage of APT effect

Table 2 Starting points and boundaries of all fit parameters of the three-pool Lorentzian fit.

	Start	Lower	Upper
Z_{base}	0.5	0.5	1
A_{water}	0.8	0	1
Γ_{water}	1	0.1	2.5
δ_{water}	0	-1	1
A_{MT}	0.1	0	1
Γ_{MT}	5	3	100
δ_{MT}	0	-0.5	0.5
A_{amide}	0.1	0	1
Γ_{amide}	1	1	1.5
δ_{amide}	3.5	3.3	3.7

The chemical shift δ and FWHM Γ are given in ppm
 Γ FWHM, δ chemical shift, *MT* magnetization transfer

nonresponse indicates no change or some alteration to individual malignant cells, but no reduction in overall cellularity compared to pretherapy core biopsy. We grouped grades 1 and 2 together as nonresponders, grades 3 and 4 as partial responders, and grade 5 as complete responders.

Statistical analysis

Statistical analysis was performed using an unpaired Mann-Whitney test (GraphPad Prism, GraphPad Software, San Diego, CA, USA), with a two-tailed distribution to show statistical difference ($\alpha = 0.05$) between the APT signal pre-NAC and after the first cycle of NAC.

A Kruskal-Wallis test with a post-hoc Dunn's multiple comparison test was used to assess statistical difference in APT signal between the groups with different pathological responses (nonresponders, partial responders, and complete responders).

Results

Data analysis

Figure 1c and d present calculated color APT maps manually overlaid on the image of the DCE series before (Fig. 1c) and after (Fig. 1d) the first cycle of NAC treatment. Within this tumor, a reduced amide signal of 21% in the APT map was observed after the first cycle of NAC.

An exemplary three-pool Lorentzian fit is depicted in Fig. 2a. The acquired data points from the tumor ROI (green circle in Fig. 1c) are shown as blue dots representing the Z-spectrum magnitude at the 32 frequency offsets, the water fit as a yellow line, the MT fit as a green line, the APT fit as a purple line, and the full fit consisting of the three fits in orange. Figure 2b shows the corresponding Z-spectrum within the tumor before (blue line) and after the first cycle of NAC treatment (red line) based on the 32 frequency offsets from the same case as in Fig. 1. Figure 2c is the insert of the dashed box in Fig. 2b, presenting the Lorentzian fit for

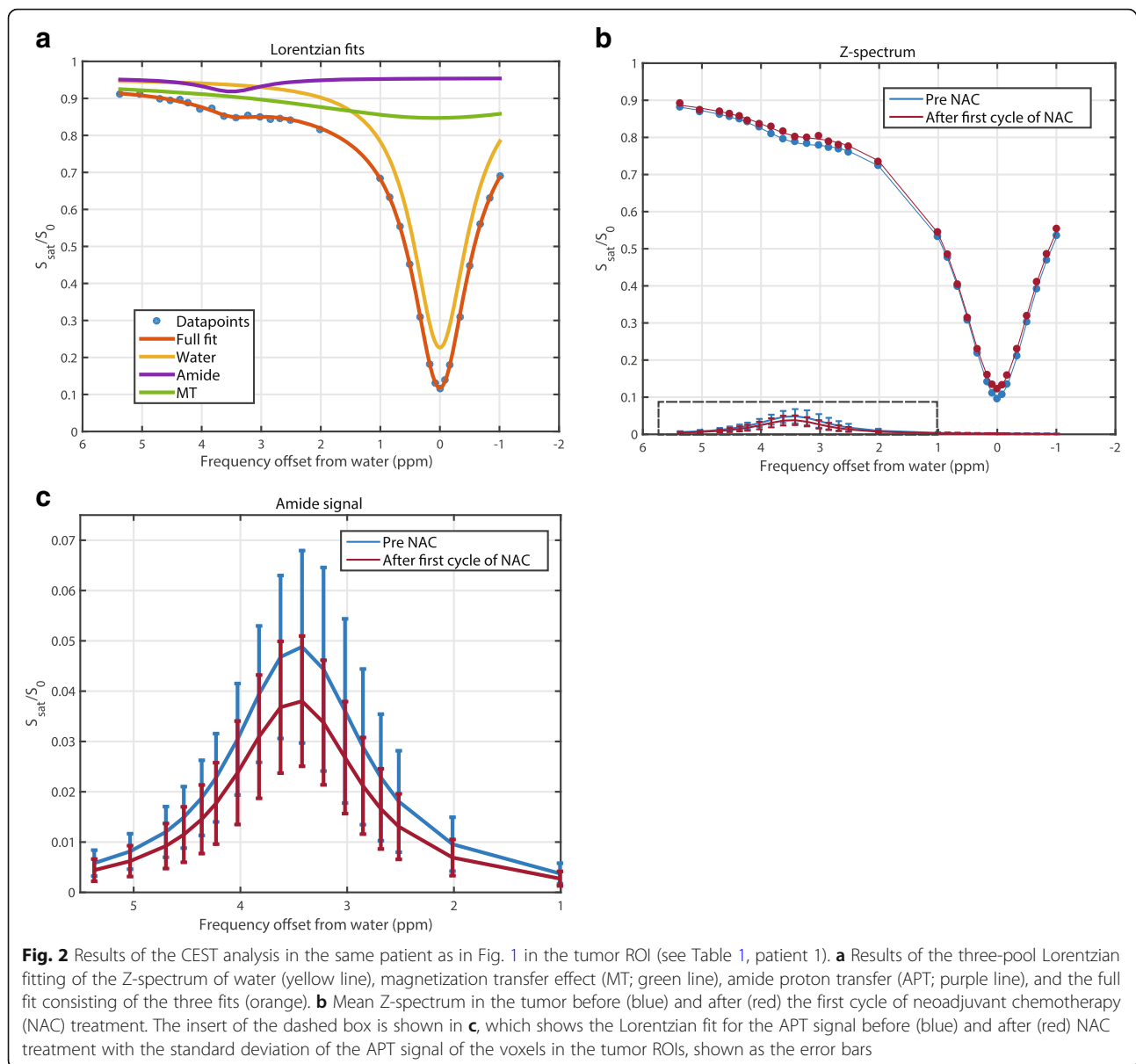
the APT signal before (blue) and after (red) NAC treatment. The 21% decrease in APT signal after the first cycle of NAC treatment can be observed.

The mean and standard deviation of the APT signal inside the tumor before and after the first cycle of NAC for all the ten lesions, together with the pathological response, are shown in Table 3. The asterisks in Table 3 indicate a significant difference comparing the APT signal before and after the first cycle of NAC treatment of each patient. Table 3 is further visualized in Fig. 3 where the nonresponders are shown in red, the partial responders in blue, and the complete responders in green. The dashed lines in Fig. 3 indicate the absence of a change in the APT signal before and after the first cycle of NAC treatment.

Normalized changes in APT signal after the first cycle of chemotherapy with pre-NAC APT signal normalized to 1 for all the tumors can be observed in Fig. 4. The one-slice approach (slice with largest tumor diameter; Fig. 4a) was compared with the change in the APT signal in the whole tumor (Fig. 4b). A distinction between the mean of the nonresponders (bright red line), the mean of the partial responders (bright blue line), and the mean of the complete responders (bright green line) is visible. Each blurred line in the backgrounds represents a different patient and the standard deviation in each group is shown as error bars. Note that the distinction between the partial responders and complete responders in the single-slice approach is clearer than in the change of APT signal in the whole tumor.

Statistical analysis

Based on the 3D whole-tumor analysis, six out of the ten lesions showed a significant change in the APT signal in the tumor, where two out of three complete responders (patients 1 and 4) showed a significant difference ($P < 0.0001$ for both patients; Table 3). The third complete responder, patient 7, showed no significant difference ($P = 0.5259$). Of the partial responders, three lesions (patients 2 and 3R and 3L) also showed a significant difference in APT signal ($P = 0.0458$, $P = 0.0004$, and $P = 0.0003$, respectively), whereas the other partial responders (patients 6 and 8) showed no significant differences ($P = 0.4135$ and $P = 0.4170$, respectively). One nonresponder showed a significant difference (patient 9, $P < 0.0001$) while the other nonresponder showed no statistical difference between the APT signal before and after the first cycle of NAC (patient 5, $P = 0.5749$). However, note that both nonresponders showed an increase in APT signal while the other responders (patient 8 as an exception) showed a decrease in the APT signal, suggesting that the nonresponders can be differentiated quite well from the responders based on the direction of the change in the APT signal.



The Kruskal-Wallis test with the post-hoc Dunn's multiple comparison test revealed no significant difference in the change of APT signal after the first cycle of NAC ($P = 0.1057$) between the three different pathological responses.

Discussion

In this preliminary study, the potential for using CEST at 7 T to monitor treatment effects in breast cancer was evaluated. We demonstrated that amide CEST signals can be measured in breast cancer before and after the first cycle of NAC. Significant differences in the APT CEST MRI signal were observed ($P < 0.05$) in six out of ten breast tumors. For the direction of the change in APT signal, the nonresponders (patients 5 and 9)

showed an increase in APT signal whereas the other patients (except patient 8) showed a decrease in the APT signal. A larger patient population is required for a more comprehensive analysis of change in APT signal in relation to pathological response.

Animal studies [27, 12] demonstrated increased APT effects in tumors compared with healthy tissue, and Salhotra et al. attributed this effect to increased cellular proliferation and subsequent accumulation of defective proteins [27, 28]. In breast tumors, Dula et al. [13] observed changes in the APT signal and attributed this to changes in the concentration of proteins and peptides or in the amide proton exchange rates, influenced by a change in pH, and perhaps T_1 [12, 29–33] due to therapy effects. Remarkably, the nonresponders in this

Table 3 Mean amide proton transfer (APT) signal in the tumor before and after the first cycle of neoadjuvant chemotherapy (NAC)

Patient	Pathological response	Mean (\pm SD) APT signal before NAC	Mean (\pm SD) APT signal after the first cycle of NAC	Delta mean APT signal	P value ^a
1	5	0.0494 (\pm 0.0062)	0.0388 (\pm 0.0046)	-0.0106	< 0.0001*
2	3	0.0319 (\pm 0.0046)	0.0311 (\pm 0.0056)	-0.0008	0.0458*
3R	4	0.0289 (\pm 0.0055)	0.0231 (\pm 0.0046)	-0.0058	0.0004*
3L	4	0.0189 (\pm 0.0020)	0.0149 (\pm 0.0034)	-0.0040	0.0003*
4	5	0.0420 (\pm 0.0098)	0.0275 (\pm 0.0043)	-0.0145	< 0.0001*
5	2	0.0132 (\pm 0.0037)	0.0140 (\pm 0.0040)	+0.0008	0.5749
6	4	0.0272 (\pm 0.0049)	0.0229 (\pm 0.0053)	-0.0043	0.4135
7	5	0.0254 (\pm 0.0056)	0.0252 (\pm 0.0043)	-0.0002	0.5259
8	3	0.0319 (\pm 0.0068)	0.0326 (\pm 0.0054)	+0.0007	0.4170
9	2	0.0381 (\pm 0.0045)	0.0465 (\pm 0.0072)	+0.0084	0.0001*

^aUnpaired Mann-Whitney test with two-tailed distribution

*Significant difference

preliminary study showed an increase in APT signal after the first cycle of NAC, which possibly hints at a continuing increase in the concentrations of proteins and peptides since the tumor was not affected by the NAC treatment. However, the increase in APT signal in the tumor is likely related to a combination of all the above-mentioned effects. Assuming these processes occur at the core of the tumor, the largest expected change in the APT signal would be at that location. This could explain the larger APT increase observed in the single-slice (with largest tumor diameter) analysis compared to the 3D whole-tumor volume analysis. (Fig. 4). As for the single-slice approach, the core contributes relatively more to the APT signal resulting in a larger mean change in APT signal compared with the mean change in APT signal of the whole tumor. It also seems that in the single-slice approach the distinction between the partial responders and the complete responders becomes clearer, hinting at a more linear distribution of change in APT signal for the

three response groups. Further research needs to be performed to examine if the single-slice approach results in a better distinction between the different response groups. Although a single-slice approach could save scan time or allow for more frequency offsets in the same scan time, caution is needed as it may be prone to unwanted interinstitutional variations due to differences in slice selection.

Although patient 7 was a complete responder, the tumor APT signal change (Fig. 3) was located in the middle of the partial responders (blue), suggesting the same change in APT signal as the partial responders. Interestingly, this was the only triple negative tumor from the three complete responders. Triple negative tumors feature a unique microenvironment distinct from that of other subtypes [34, 35], possibly explaining the different APT signal in this type of tumor; however, this observation remains to be confirmed.

Due to the small sample size ($n = 10$) we did not correct for age or menstrual cycle effects, which are known

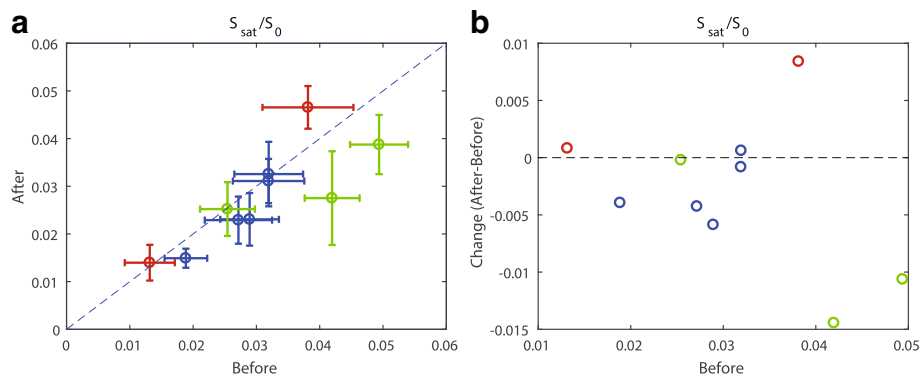


Fig. 3 Mean APT signal and standard deviation within the ROI (tumor) for all ten lesions. **a** The mean APT signal after the first cycle of NAC is plotted versus the mean APT signal before the start of NAC for the nonresponders (red), partial responders (blue), and complete responders (green). **b** The mean change in APT signal is plotted versus the mean APT signal before NAC. The dashed lines in both **a** and **b** indicate the absence of a change in APT signal before and after the first cycle of NAC treatment

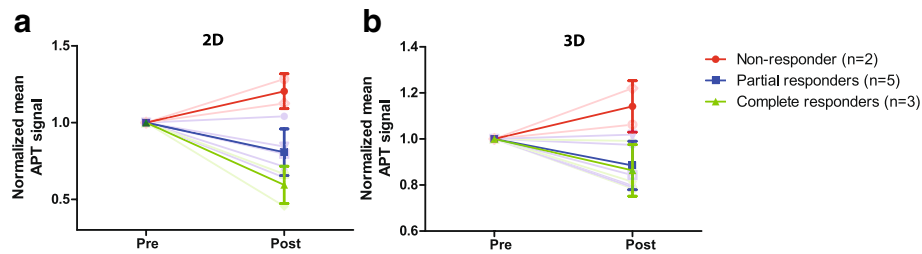


Fig. 4 Normalized changes in amide proton transfer (APT) signal after the first cycle of neoadjuvant chemotherapy in the slice with the largest tumor diameter **a** and in the whole tumor **b**. The mean of the nonresponders (bright red line), partial responders (bright blue line), and complete responders (bright green line) on top of the change in APT signal of all the lesions (transparent lines in the background), where each line represents a different lesion. The standard deviation in each group is shown as error bars

to affect the breast density. The water content of the breast parenchyma particularly changes during the menstrual cycle [36], possibly influencing the CEST effect [16, 17]. Additionally, all patients in this study received NAC treatment which is known to influence the menstrual cycle.

The overall calculated APT contrast can also be influenced by the degree of fat suppression. We used RF and gradient spoiling to reduce lipid artefacts. However, insufficient fat suppression in the tumor may have resulted in an underestimation of the CEST amplitude [37], possibly affecting the change in APT signal.

CEST MRI is sensitive to the B_1^+ field, since different exchanging groups are affected by the B_1^+ . Variation in B_1^+ may cause more contrast from slower (or faster) exchanging species. We were interested in the APT CEST MRI signal generated by the slow exchanging amide protons, and the optimal B_1^+ for detecting this exchange is approximately $1 \mu\text{T}$ [38]. The peak B_1 amplitude in this study was set to $2 \mu\text{T}$ to account for B_1 loss due to the hardware setup. The unilateral setup consisted of a quadrature RF coil placed in front of the breast, while the bilateral setup was an exact copy of this coil, only for both breasts. This setup led to a decrease in B_1 , varying from 60% in the front of the breast to 50% towards the pectoralis major. The sequence was optimized to achieve an acquired B_1 of approximately $1 \mu\text{T}$ throughout the breast. Therefore, the location of the tumor can possibly influence the measured change in the APT CEST signal. In this study, we assumed that the location of the tumor was the same between the two measurements receiving the same amount of B_1 and therefore not influencing the measured change in the APT CEST signal. Several B_1^+ inhomogeneity correction methods have been proposed [25, 39, 40] to improve the CEST images. These methods, however, require an accurate B_1 map or acquisition at multiple B_1 amplitudes. Due to limited scan time this was unfortunately not possible in this study. Another solution to deal with B_1 inhomogeneity would be a new design for the coil setup at 7 T where a

homogeneous B_1 field can be achieved. For example, the use of dipole antennas has been shown to achieve this in body imaging [41]. These methods for improving the B_1 field could be good options for future studies to further improve the quality of the APT maps of the breast.

It would be interesting to translate these findings to the clinical field strength of 3 T. Klomp et al. [14], however, compared APT CEST MRI at 3 T with 7 T and found that the variance of noise in measurements at 3 T was large (i.e., approximately 5% of CEST effects when compared with the water signal, larger than the alterations in CEST effects we have observed in our study), thereby limiting the ability to discern subtle changes during, for example, first-line therapy. At 7 T, however, the increased SNR and increased spectral resolution enabled a fourfold reduction in the noise of the observed APT CEST compared with 3 T. Due to the inherently small CEST signal, at the moment changes within these CEST effects seem challenging to detect at 3 T. Fortunately, 7 T has been Food and Drug Administration (FDA) approved and thereby will likely become available to more hospitals.

Predictive biomarkers are critical for the evaluation of neoadjuvant therapies, as well as the effect of novel targeted agents intended to be incorporated into neoadjuvant therapy [42]. The potential for high-field-strength CEST MRI of the breast as a biomarker for the evaluation of NAC response is promising, as is the capability to noninvasively detect changes in protein and peptide levels. These may play a key role in understanding breast tumor progression and response to treatment [19].

Conclusions

In a small group of breast cancer patients, this preliminary study shows the feasibility of using APT CEST MRI at 7 T as a noninvasive biomarker to predict the effect of neoadjuvant chemotherapy in an early stage of treatment. This can be useful in personalized breast cancer treatment planning.

Abbreviations

APT: Amide proton transfer; CEST: Chemical exchange saturation transfer; CNR: Contrast to noise ratio; DCE: Dynamic contrast-enhanced; MRI: Magnetic resonance imaging; MT: Magnetization transfer; NAC: Neoadjuvant chemotherapy; NOE: Nuclear Overhauser effect; RF: Radiofrequency; ROI: Region of interest; SNR: Signal to noise ratio; T: Tesla

Acknowledgements

We thank the Dutch Cancer Society (Alpe d'Huzes project nr: UU 2013-6302) and the NWO (VENI grant: J.P.Wijnen 016.148.002) for financial support.

Funding

Dutch Cancer Society (Alpe d'Huzes project nr: UU 2013-6302) and the NWO (VENI grant: J.P.Wijnen 016.148.002).

Availability of data and materials

The datasets generated and/or analyzed during the current study are not publicly available due to privacy and legal reasons, but are available from the corresponding author on reasonable request.

Authors' contributions

The design of the study was made by JPW, DWJK, HWMvL, and PRL. EK, JPW, RAJ, and HWMvL acquired all the data. MZ and VK helped EK analyze the CEST data. PjvD and EK performed the histological examination on all biopsies and breast specimens after surgery. DWJK, JPW and VK assisted with developing the CEST sequence. All authors contributed to the writing of the manuscript and interpretation of the data. All authors read and approved the final manuscript.

Ethics approval and consent to participate

See 'METC nader positief besluit_09-11-2016.pdf' for the latest approval by the Medical Research Ethics Committee (METC) of the University Medical Center Utrecht.

The Medical Research Ethics Committee (METC) of the University Medical Center Utrecht confirms that it has reviewed the amendment to the study in accordance with the Dutch Medical Research Involving Human Subjects Act (WMO) and other applicable Dutch and European regulations. Based on the requirements of the WMO, the METC of the University Medical Center Utrecht hereby issues an approval of the amendment to the above mentioned study.

Consent for publication

Consent for publication was obtained from all participants in the study.

Competing interests

The authors declare that they have no competing interests.

Publisher's Note

Springer Nature remains neutral with regard to jurisdictional claims in published maps and institutional affiliations.

Author details

¹Department of Radiology, University Medical Center Utrecht, Utrecht, The Netherlands. ²Max Planck Institute for Biological Cybernetics, Tübingen, Germany. ³Department of Medical Oncology, Academic Medical Centre Amsterdam, Amsterdam, The Netherlands. ⁴Department of Pathology, University Medical Center Utrecht, Utrecht, The Netherlands.

Received: 14 December 2017 Accepted: 10 May 2018

Published online: 14 June 2018

References

- Loibl S, Von Minckwitz G, Blohmer J, et al. Surgical procedures after neoadjuvant chemotherapy in operable breast cancer: results of the GEPAR DUO trial. *Ann Surg Oncol*. 2006;13(11):1434–42.
- Kaufmann M, Hortobagyi GN, Goldhirsch A, et al. Recommendations from an international expert panel on the use of neoadjuvant (primary) systemic treatment of operable breast cancer: an update. *J Clin Oncol*. 2006;24(12):1940–9.
- Kaufmann M, Von Minckwitz G, Bear HD, et al. Recommendations from an international expert panel on the use of neoadjuvant (primary) systemic treatment of operable breast cancer: new perspectives 2006. *Ann Oncol*. 2007;18(11):1927–34.
- Kaufmann M, Von Minckwitz G, Mamounas EP, et al. Recommendations from an international consensus conference on the current status and future of neoadjuvant systemic therapy in primary breast cancer. *Ann Surg Oncol*. 2011;19:1508–16.
- Fisher B, Brown A, Mamounas E, et al. Effect of preoperative chemotherapy on local-regional disease in women with operable breast cancer: findings from National Surgical Adjuvant Breast and Bowel Project B-18. *J Clin Oncol*. 1997;15(7):2483–93.
- Bonadonna G, Valagussa P, Zucali R, Salvadori B. Primary chemotherapy in surgically resectable breast cancer. *CA Cancer J Clin*. 1995;45(4):227–43.
- Tudorica A, Oh KY, Chui SYC, et al. Early prediction and evaluation of breast cancer response to neoadjuvant chemotherapy using quantitative DCE-MRI. *Transl Oncol*. 2016;9(1):8–17.
- Harry VN, Semple SI, Parkin DE, Gilbert FJ. Use of new imaging techniques to predict tumour response to therapy. *Lancet Oncol*. 2010;11(11):92–102.
- Padhani AR, Miles KA. Multiparametric imaging of tumor response to therapy. *Radiology*. 2010;256(2):348–64.
- Wolff SD, Balaban RS. NMR imaging of labile proton exchange. *J Magn Reson*. 1990;86(1):164–9.
- Van Zijl PCM, Zhou J, Mori N, Payen JF, Wilson D, Mori S. Mechanism of magnetization transfer during on-resonance water saturation. A new approach to detect mobile proteins, peptides, and lipids. *Magn Reson Med*. 2003;49(3):440–9.
- Zhou JY, Lal B, Wilson DA, Lartera J, van Zijl PCM. Amide proton transfer (APT) contrast for imaging of brain tumors. *Magn Reson Med*. 2003;50(6):1120–6.
- Dula AN, Arlinghaus LR, Dortch RD, et al. Amide proton transfer imaging of the breast at 3 T: establishing reproducibility and possible feasibility assessing chemotherapy response. *Magn Reson Med*. 2013;70:216–24.
- Klomp DWJ, Dula AN, Arlinghaus LR, et al. Amide proton transfer imaging of the human breast at 7T: development and reproducibility. *NMR Biomed*. 2013;26(10):1271–7.
- Zaiss M, Windschuh J, Paech D, et al. Relaxation-compensated CEST-MRI of the human brain at 7T: unbiased insight into NOE and amide signal changes in human glioblastoma. *Neuroimage*. 2015;112:180–8.
- Zaiss M, Xu J, Goerke S, et al. Inverse Z-spectrum analysis for spillover-, MT-, and T1-corrected steady-state pulsed CEST-MRI—application to pH-weighted MRI of acute stroke. *NMR Biomed*. 2014;27(3):240–52.
- Khlebnikov V, Polders D, Hendrikse J, et al. Amide proton transfer (APT) imaging of brain tumors at 7 T: the role of tissue water T1-relaxation properties. *Magn Reson Imaging*. 2017;77:1525–32.
- Khlebnikov V, Siero JCW, Wijnen J, et al. Is there any difference in amide and NOE CEST effects between white and gray matter at 7 T? *J Magn Reson*. 2016;272:82–6.
- Dula AN, Dewey BE, Arlinghaus LR, et al. Optimization of 7-T chemical exchange saturation transfer parameters for validation of glycosaminoglycan and amide proton transfer of fibroglandular breast tissue. *Radiology*. 2014;275(1):255–61.
- Van Der Velden TA, Italiaander M, Der Kemp WJM V, et al. Radiofrequency configuration to facilitate bilateral breast 31P MR spectroscopic imaging and high-resolution MRI at 7 Tesla. *Magn Reson Med*. 2015;74(6):1803–10.
- Klomp DWJ, van der Kemp WJM, Korteweg M, Wijnen JP, Van De Bosch M, Luijten PR. P MRS at 7T can be more sensitive and specific than 1 H MRS in monitoring breast cancer treatment. *Proc Intl Soc Mag Reson Med*. 2011;19:343.
- Hancu I, Govencar A, Lenkinski RE, Lee SK. On shimming approaches in 3T breast MRI. *Magn Reson Med*. 2013;69(3):862–7.
- Khlebnikov V, Geades N, Klomp DWJ, Hoogduin H, Gowland P, Mouglin O. Comparison of pulsed three-dimensional CEST acquisition schemes at 7 Tesla: steady state versus pseudosteady state. *Magn Reson Med*. 2017;77:2280–7.
- Kim M, Gillen J, Landman BA, Zhou J, Van Zijl PCM. Water saturation shift referencing (WASSR) for chemical exchange saturation transfer (CEST) experiments. *Magn Reson Med*. 2009;61(6):1441–50.
- Windschuh J, Zaiss M, Meissner J, et al. Correction of B1-inhomogeneities for relaxation-compensated CEST imaging at 7T. *NMR Biomed*. 2015;28:529–37.
- Orgston KN, Miller ID, Payne S, et al. A new histological grading system to assess response of breast cancers to primary chemotherapy: prognostic significance and survival. *Breast*. 2003;12:320–7.
- Salhotra A, Lal B, Lartera J, Sun PZ, van Zijl PCM, Zhou J. Amide proton transfer imaging of 9L gliosarcoma and human glioblastoma xenografts. *NMR Biomed*. 2008;21:489–97.

28. Adams J. The proteasome: a suitable antineoplastic target. *Nat Rev Cancer*. 2004;4(5):349–60.
29. Zhou J, Blakeley JO, Hua J, et al. Practical data acquisition method for human brain tumor amide proton transfer (APT) imaging. *Magn Reson Med*. 2008;60(4):842–9.
30. Zhou J, Tryggstad E, Wen Z, et al. Differentiation between glioma and radiation necrosis using molecular magnetic resonance imaging of endogenous proteins and peptides. *Nat Med Nature*. 2011;17(1):130–4.
31. Jones CK, Schlosser MJ, Van Zijl PCM, Pomper MG, Golay X, Zhou J. Amide proton transfer imaging of human brain tumors at 3T. *Magn Reson Med*. 2006;56(3):585–92.
32. Wen Z, Hu S, Huang F, et al. Neuroimage MR imaging of high-grade brain tumors using endogenous protein and peptide-based contrast. *Neuroimage*. 2010;51(2):616–22.
33. Zhou J, Payen JF, Wilson DA, Traystman RJ, Van Zijl PCM. Using the amide proton signals of intracellular proteins and peptides to detect pH effects in MRI. *Nat Med*. 2003;9(8):1085–90.
34. Foulkes WD, Smith IE, Reis-Filho JS. Triple-negative breast cancer. *N Engl J Med*. 2010;363:1938–48.
35. Yu T, Di G. Role of tumor microenvironment in triple-negative breast cancer and its prognostic significance. *Chinese J Cancer Res*. 2017;29(3):237–52.
36. Delille J, Slanetz PJ, Yeh ED, Kopans DB, Garrido L. Physiologic changes in breast magnetic resonance imaging during the menstrual cycle: perfusion imaging, signal enhancement, and influence of the T1 relaxation time of breast tissue. *Breast J*. 2005;11(4):236–41.
37. Zhang S, Keupp J, Wang X, et al. Z-spectrum appearance and interpretation in the presence of fat: influence of acquisition parameters. *Magn Reson Med*. 2017;0:1–7.
38. Zu Z, Li K, Janve VA, Does MD, Gochberg DF. Optimizing pulsed-chemical exchange saturation transfer imaging sequences. *Magn Reson Med*. 2011;66(4):1100–8.
39. Singh A, Cai K, Haris M, Hariharan H. On B1 inhomogeneity correction of in vivo human brain glutamate chemical exchange saturation transfer contrast at 7T. *Magn Reson Imaging*. 2013;69:818–24.
40. Khlebnikov V, Windschuh J, Siero JCW, et al. On the transmit field inhomogeneity correction of relaxation-compensated amide and NOE CEST effects at 7 T. *NMR Biomed*. 2017;30:e3687.
41. Raaijmakers AJE, Italiaander M, Voogt IJ, et al. The fractionated dipole antenna: a new antenna for body imaging at 7 Tesla. *Magn Reson Med*. 2016;75(3):1366–74.
42. Rubovszky G, Horváth Z. Breast cancer: recent advances in the neoadjuvant treatment of breast cancer. *J Breast Cancer*. 2017;20(2):119–31.

Ready to submit your research? Choose BMC and benefit from:

- fast, convenient online submission
- thorough peer review by experienced researchers in your field
- rapid publication on acceptance
- support for research data, including large and complex data types
- gold Open Access which fosters wider collaboration and increased citations
- maximum visibility for your research: over 100M website views per year

At BMC, research is always in progress.

Learn more biomedcentral.com/submissions

